Light-powered reactivation of flagella: towards self-sustained movement of artificial cells

R. Ahmad[1†], C. Kleineberg[2†], Y. Su[1], S. Goli Pozveh[1], A. J. Bae[1‡], E. Bodenschatz[1,3], K. Sundmacher[2,4], T. Vidakovich-Koch[2*], A. Gholami[1*]

[1]Max Planck Institute for Dynamics and Self-Organization, Am Fassberg 17, 37077 Göttingen, Germany
[2]Max-Planck Institute for Dynamics of Complex Technical Systems, Sandtorstraße 1, 39106 Magdeburg, Germany
[3]Institute for Dynamics of Complex Systems, Georg-August-University Göttingen, 37073 Göttingen, Germany
[4]Otto von Guericke University, Universitätsplatz 2, 39106 Magdeburg, Germany

***For correspondence:** azam.gholami@ds.mpg.de; vidakovic@mpi-magdeburg.mpg.de
[†]These authors contributed equally to this work.
[‡]**Present address:** Department of Biomedical Engineering, University of Rochester, USA.

Abstract

Artificial systems capable of self-sustained directed movement are of high interest with respect to development of many challenging applications including medical treatments but also technical applications. The bottom-up assembly of such systems in the context of synthetic biology is still a challenging task. Here, we demonstrate the biocompatibility and efficiency of an artificial light-driven energy module and a motility functional unit by integrating light-switchable photosynthetic vesicles with demembranated flagella, thereby supplying ATP for dynein molecular motors upon illumination. Flagellar propulsion is coupled to its beating frequency and the dynamic synthesis of ATP triggered by energy of light, enabled us to control beating frequency of flagella as a function of illumination. Light-powered functionalized vesicles integrated with different biological building blocks such as bio-polymers and molecular motors may contribute to bottom-up synthesis of artificial cells that are able to undergo motor-driven morphological deformations and exhibit directional motion in a light-controllable fashion.

1 Introduction

Bottom-up synthetic biology is an emerging field of science focusing on engineering of life-like structures. These artificial constructs mimic some of the essential life processes like reproduction, growth, motility, etc. Reconstitution of each of these processes is quite complex, so the bottom-up synthetic biology focuses at first to sub-systems (functional modules), which are hand-tailored to partially or entirely mimic some of essential life processes (1–3). Later on these functional modules can be combined to build up higher hierarchical structures. With this respect, artificial systems capable of moving forward are highly attractive for different applications. Examples are smart drug delivery vehicles, or so-called designer immune cells which would be capable of detecting and moving towards a chemical signal or tumor (4). In these applications motility is only one of functionalities, but even its reconstitution is quite challenging since it embraces, not

only the assembly of molecular motors (a motility functional module) which enable movement but also the delivery of energy-rich ATP molecules (energy functional module).

In nature different motility mechanisms are evolved, including polarized assembly and disassembly of bio-polymers for directional motion of amoboid cells (5, 6), or propulsion powered by ancient organelles cilia and flagella which perform whip-like motion (7) to provide motility for primitive eukaryotic cells living in an aqueous environment (8). Cilia and flagella are composed of a microtubule-based structure called axoneme which is covered by a plasma membrane (9, 10). Nine microtubule doublets, each formed of a complete A-microtubule and an incomplete B-microtubule, are cylindrically arranged around two microtubule singlets in the middle. The diameter of an axoneme is around 200 nm, and the adjacent microtubule doublets are spaced 30 nm away from each other (11). The functionality and structural properties of cilia and flagella are the same and can be classified as motile (9+2) and immotile sensory (9+0) cilia. To date, more than 250 constituent proteins have been found to contribute to the highly ordered and precisely assembled structure of axoneme (12). The microtubule doublets and the dynein molecular motors are the most important components of axonemes (13, 14). Axonemal dyneins are highly specific for ATP as substrate (15, 16). In the presence of ATP, dynein molecular motors, which are statically bound to the A tubules of each doublet, attach themselves transiently to the B tubules and generate internal stresses to displace adjacent microtubules relative to each other. However, since microtubule doublets are mechanically connected to the neighboring doublets and cannot slide freely, this sliding force is converted into a bending movement. Since the bottom-up reconstitution of flagella is of significant complexity, we isolated this functional module from green algae *Chlamydomonas reinhardtii*. The isolated motility functional module has all infrastructure required for a directed movement, but ATP fuel is lacking. Therefore an ATP regeneration module is required for a self-sustained system.

With respect to this, we recently reviewed (1) different strategies for ATP regeneration in the context of bottom-up synthetic biology and we reported on different types of energy functional modules (17, 18). They are basically utilizing either chemical (17) or light energy (18) to regenerate ATP out of ADP. The later system appears especially promising for coupling with such bottom-up applications which rely only on ATP as an energy carrier and do not involve NADH (NAD(P)H) reductive power, like in the case of motility. The light energy driven ATP regeneration is not novel; for mimicking natural photophosphorylation, a series of artificial systems have been constructed to capture the energy of light and move protons across the membranes (19). Simple prototypical systems, which combine light-driven proton pumps with the F_OF_1-ATP synthase in liposomes have been demonstrated already in the early 70s, the motivation being to develop in vitro models for the mechanistic understanding of F_OF_1-ATP synthase. By varying several different types of rhodopsins and F_OF_1-ATP synthases as well as of the lipid composition, the productivity of these assemblies was improved as shown by us (18) and other authors (20–23). Recently some examples showing coupling of light-driven ATP regeneration module with energy intensive tasks like CO_2 fixation (24) and actin contractions (25) as well as protein synthesis (26) were demonstrated. However, there was no study demonstrating self-sustained system showing directed movement driven

by ATP.

In this contribution, we integrated a light-switchable bottom-up assembled ATP regeneration module with a motility functional unit which was isolated from green algae *Chlamydomonas reinhardtii*. Combination of these two modules allows us a dynamic synthesis of ATP, controlling beating frequency and thereby swimming trajectory of flagella as a function of illumination. Our integrated system has potential application in ATP-dependent motility assays, which aim to reconstitute motor-driven motion and force generation inside a synthetic cell, with the ultimate goal of achieving light-controllable switch between motile and immotile state of an artificial cell.

2 Results

We engineered switchable photosynthetic liposomes (∼150 nm in diameter) as energy modules to generate ATP upon illumination. To convert light into energy, we co-reconstituted two purified transmembrane proteins namely, Bacteriorhodopsin (bR) and EF_OF_1 ATP synthase from E. coli. Upon illumination, Bacterorhodopsin pumps proton inside the vesicles interior, establishing a proton motive force that drives ATP synthase to catalyze the convertion of ADP to ATP (Fig. 1A). Both enzymes are isolated according to a standard procedure earlier described by Ishmukhametov, Galkin, and Vik (27) and Oesterhelt (28). Their purity is checked by SDS-PAGE analysis (SI, Fig. S1). bR is reconstituted in form of membrane patches to avoid material loss during solubilization. We recently showed that (18) the usage of monomeric, detergent-solubilized bR for reconstitution is also possible and will lead to functional ATP regeneration module. Both enzymes are co-reconstituted into preformed phosphatidylcholine unilamellar vesicles using Triton X-100 as detergent, similar to the method described by Fischer and Gräber (29) for ATP synthase reconstitution. Liposomes are prepared using the extrusion method. The size of vesicles before and after reconstitution is checked using Dynamic Light Scattering (DLS). DLS data confirm an average vesicle diameter of 150 nm (SI, Fig. S2). A separated assay for each transmembrane protein respectively further proves their functionality. bR proton pumping and intravesicular acidifidication interior is detected using pyranine as internal probe (SI, Fig. S3). The activity of ATP synthase is determined in an acid-base transition experiment (SI, Fig. S4). ATP production in the co-reconstituted module under illumination is measured using the luciferin/luciferase assay (Fig. 1B). The achieved maximal rate of 4.5 µmol ATP $(\mathrm{mgEF_OF_1})^{-1}\mathrm{min}^{-1}$ is high compared to literature work. An overview of different light-driven and chemically-driven ATP regeneration modules and their ATP production rates can be found in our recent article (1). As the ATP production rates depend on many factors such as the bR/ATP synthase ratio per liposomes, the ADP concentration or the power of the light source (19, 21–23, 30), a straightforward comparison between different results in literature is difficult.

Next, we coupled the light-driven ATP regeneration module with flagella (∼10 μm in length) isolated from green algae *C. reinhardtii* (31), as schematically displayed in Fig. 2A. Upon illumination, ATP is produced which powers the activity of axonemal dyneins, converting chemical energy to mechanical work by sliding neighboring microtubule doublets relative to each other. However,

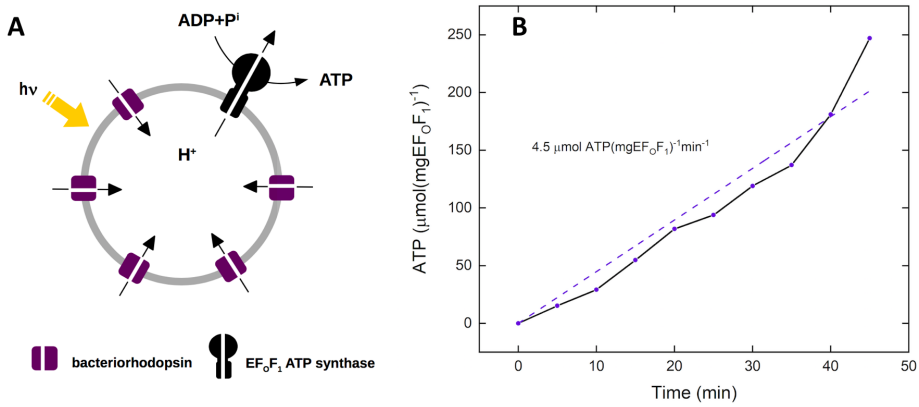

Fig. 1: Light-driven ATP production. A) Schematic representation of light-driven ATP synthesis in lipid vesicles. EF_OF_1 ATP synthase uses the electrochemical gradient generated by bacteriorhodopsin to synthesize ATP from ADP and Pi. B) Measurement of light-driven ATP production over time. The maximal rate of 4.5 µmol ATP $(mgEF_OF_1)^{-1}min^{-1}$ is determined by linear regression.

due to mechanical constrains, MT doublets are not free to slide, instead sliding will be converted to rhythmic bending deformations that propagate along the contour length of axonemes with a frequency which depends on ATP concentration (supplemental Video 1). As shown in Fig.2B and 2C, higher ATP concentrations are produced by illuminating the energy module for a longer period of time. Interestingly, we observed that even after 1 min of illumination with microscope light, 650 nM ATP was produced which was sufficient to reactivate axonemes with a beating frequency of around 20 Hz. Our quantitative analysis of beating frequency of reactivated axonemes confirm that they beat faster at higher ATP concentrations generated by longer illumination periods (Fig. 2D). These results are in agreement with the frequency trend reported by Geyer et.al. (32). However, we observed that axonemes beat even at ATP concentrations well below 30 µM. We performed experiments with fluorescently labeled vesicles to examine possibility of vesicle accumulation in the vicinity of axonemes which can locally generate higher ATP concentrations upon illumination. However, these experiments did not confirm any significant higher fluorescent intensity in the area close to the axonemes.

Figure 3A and B shows exemplary oscillatory motion of an axoneme in response to ATP generated by light-driven energy module (supplemental Video 2). We observed curvature waves propagating with frequency of up to 72 Hz along the contour length (Fig. 3C). To quantify the oscillatory motion of axonemes, we first tracked filaments using gradient vector flow (GVF) technique (33, 34) and measured the curvature of the mean shape (see Materials and Methods). We translate and rotate configurations of an actively beating axoneme such that the basal end defined as $s = 0$ is at position $(0, 0)$ and the tangent vector at the basal end is orientated in the $\hat{x}$ direction (Fig. 3D). Figure 2D illustrates that curvature of the mean shape does not significantly depend on ATP concentration

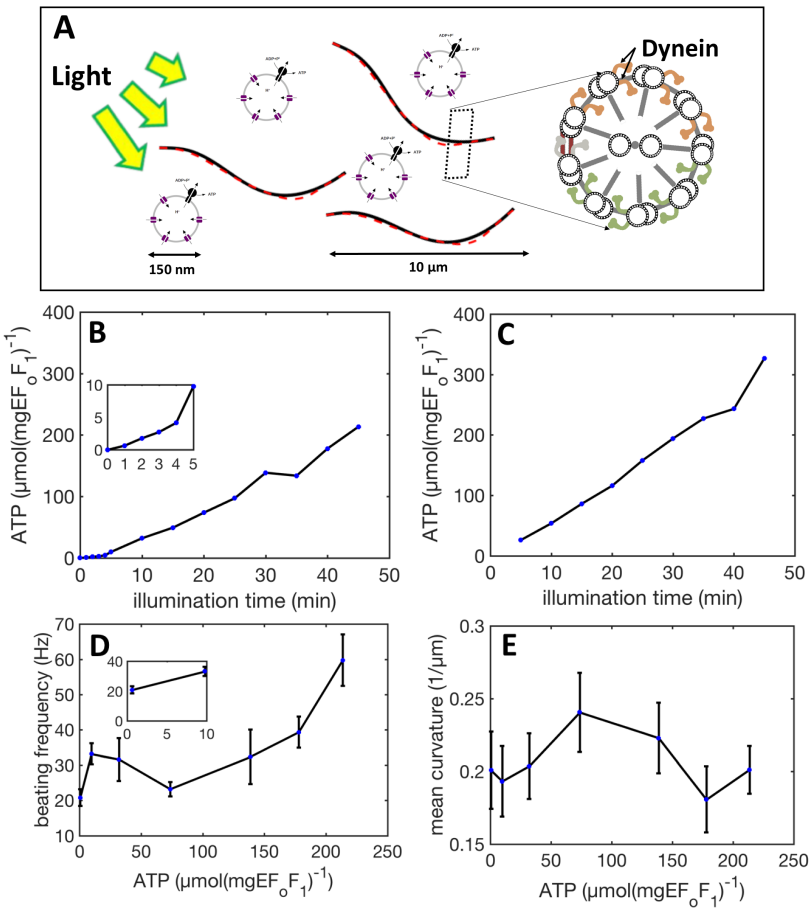

Fig. 2: A) Schematic representation of light-powered energy module integrated with isolated flagella. Functionalized liposomes are illuminated for different times, generating ATP concentrations up to 330 µM. B) Illumination under microscope light (5W) and C) illumination with a LED lamp (50 W). Both light sources are located 25 cm away from the sample. Inset shows ATP production in the time interval 0 to 5 min of illumination. D) Axonemes beat faster at higher ATP concentrations produced by longer illumination of energy module under microscope light. Inset shows that axonemes beat even at small ATP concentrations. E) Mean curvature of axoneme's mean shape does not significantly depend on ATP concentration.

produced upon illumination (32).

To describe shape dynamics of axonemes, we followed principal mode analysis introduced by Stephens et al. (35) (see Materials and Methods). First, tracked axonemes obtained by GVF technique (33, 34) was used to compute $\theta(s,t)$ which is the angle between the local tangent vector and $\hat{x}$ axis (see Fig. 3A). Next, we calculated covariance matrix $C(s,s')$ of fluctuations in angle which has only a small number of nonzero eigenvalues. The color map of

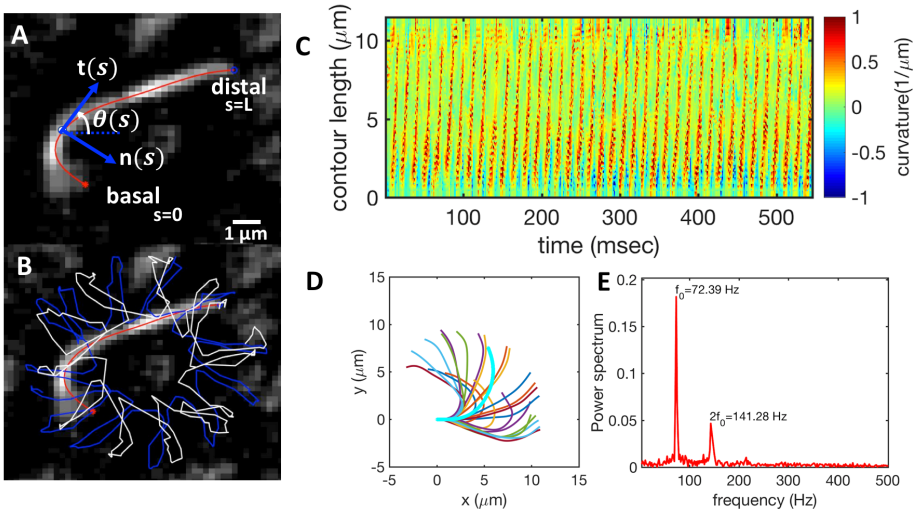

Fig. 3: Reactivation of axonemes by light-driven energy module. (A) Actively beating axoneme in the presence of 213 μM ATP produced upon illumination of energy module for 45 min by microscope light. (B) As axoneme beats with frequency of 72 Hz, it rotates with slower frequency of 2 Hz. Blue and white trajectories show the trace of basal and the distal end, respectively. (C) Curvature waves propagating along the contour. (D) Axoneme's shape at different time points are translated and rotated such that basal end is at $(0, 0)$ and the orientation of the tangle vector at the basal end is in the $\hat{x}$ direction. (E) Power spectrum showing dominant peaks at $f_0 = 72$ Hz and second harmonic of $\sim 2f_0$.

this matrix presented in Fig. 4A shows that $C(s, s')$ has an effective reduced dimensionality. As shown by Stephens et al. (35) for C.elegance, only four eigenvectors $V_n(s)$ $(n = 1, .., 4)$ corresponding to the first four largest eigenvalues of covariance matrix are enough to describe axoneme's shape with high accuracy (Fig.4G, H and I). The first two motion amplitudes $a_1(t)$ and $a_2(t)$ are shown in Fig. 4C, D and the corresponding probability density is presented in Fig. 4B (see Materials and Methods). Considering reactivated axonemes as an example of a self-sustained biological oscillator, it is possible to define a phase which facilitates quantitative analysis. To present instantaneous state of an oscillator, we consider the stable limit cycle that forms in $a_1 - a_2$ plane, and define phase as a monotonically increasing function $\phi(t)$ (Fig. 4B, F). For a given limit cycle, phase ϕ rotates uniformly in the phase space such that $d\phi/dt = 2\pi f_0$, where f_0 is the autonomous beating frequency of axoneme (Fig. 4F).

3 Discussion

Our experiments demonstrate that light-switchable photosynthetic liposomes can drive ATP-dependent activity of axonemal dyneins which serve as tiny protein machinery converting chemical energy into mechanical work in the form of a rhythmic beating pattern. We used energy of light for dynamic synthesis

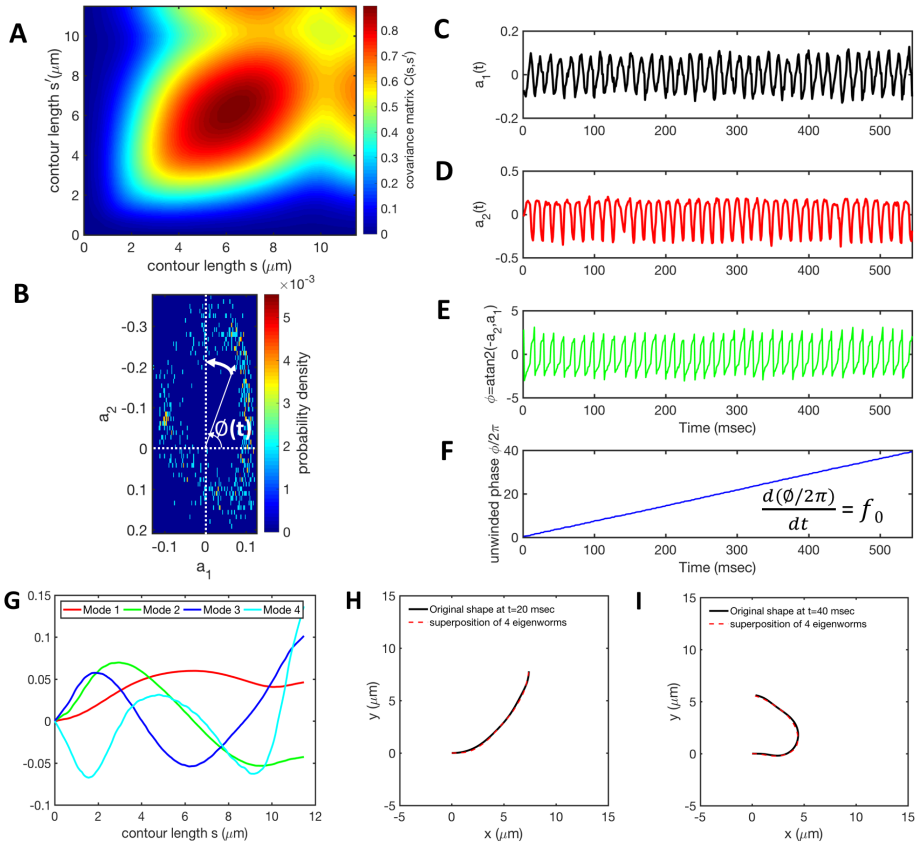

Fig. 4: A) The covariance matrix $C(s, s')$ of fluctuations in angle $\theta(s, t)$. B) Probability distribution of the first two shape amplitudes $p(a_1(t), a_2(t))$. The phase angle of the axoneme as an oscillator is defined as $\phi(t) = \text{atan2}(-a_2(t), a_1(t))$. (C-D) Time evolution of the first two dominant shape amplitudes $a_1(t)$ and $a_2(t)$ showing regular oscillations at frequency of 72 Hz. E-F) We observe a linear growth in dynamics of $\phi(t)$, indicating steady rotation in $a_1 - a_2$ plane presented in part B. Note that $d\phi/dt = 2\pi f_0$ where f_0 is the beating frequency of axoneme. G) Four eigenvectors corresponding to four largest eigenvalues of matrix $C(s, s')$. H-I) Superposition of four eigenmodes presented in part G with coefficients $a_1(t)$ to $a_4(t)$, can reproduce shape of axoneme with high accuracy.

of ATP, allowing us to control beating frequency of axonemes as a function of illumination. Functionalized artificial liposomes, capable of continuous production of ATP by shining light as external stimulus, can serve as an efficient energy module for variety of in vitro microtubule- and actin-based motility assays where molecular motors are actively engaged in generating and sustaining active stresses in the network. Our developed scheme could serve as a potential platform to encapsulate constituent elements such as actin, microtubules and various regulatory components inside functionalized lipid vesicles, providing ATP in an optical-controllable fashion. ATP-driven motor activity in filamen-

tous biopolymer networks is expected to generate active forces, driving morphological deformations in liposomes, and will further contribute to achieving the challenging goal of designing an artificial cell from the bottom-up approach.

4 Material and Methods

Expression and purification of membrane proteins

Purple membrane was isolated from Halobacterium salinarium (strain S9) as described by Oesterhelt (28). His-tagged E. coli F_OF_1-ATP synthase (EF_OF_1) was expressed from the plasmid pBWU13-βHis in the E. coli strain DK8 (ΔuncBEFHAGDC) and purified by Ni-NTA affinity chromatography as previously described by Ishmukhametov, Galkin, and Vik (27)

Preparation of lipid vesicles for light-driven ATP production

Vesicles were formed by film rehydration method followed by extrusion. 10 mg of dissolved phosphatidylcholine lipid was deposited in a glass vial and solvent was removed using a gentle stream of nitrogen. Thin lipid films were rehydrated in HMDEKP buffer (30 mM HEPES-KOH, 5 mM $MgSO_4$, 1 mM DTT, 1 mM EGTA, 50 mM potassium acetate, 1 % PEG, pH 7.4) to a final concentration of 10 mg/ml by vortexing. To transform multilamellar vesicles into unilamellar vesicles, the suspension was subjected to 5 freeze-thaw cycles. Each cycle consisted of freezing in liquid nitrogen, thawing in a 35°C water bath and vortexing for 30 s. Suspensions were extruded 11 times through a 100 nm pore size polycarbonate membrane (Whatman) to form uniform vesicles.

Co-reconstitution of EF_OF_1-ATP synthase and bR

100 µL of preformed vesicles were mixed with 0.1 µM EF_OF_1-ATP synthase and 99 µM bR in form of membrane patches. 0.8 % Triton X-100 was added under vortexing to partially solubilize the vesicles. After 15 minutes incubation in the dark under gentle shaking, 80 mg of wet SM-2 Bio-Beads were added and the solution was incubated for further 60 minutes under constant shaking in the dark.

Light-induced ATP production

For measurement of light-induced ATP production, 25 µL of co-reconstituted vesicles were diluted in 250 µL of HMDEK buffer (30 mM HEPES-KOH, 5 mM $MgSO_4$, 1 mM DTT, 1 mM EGTA, 50 mM potassium acetate, pH 7.4) supplemented with 1% (w/v) polyethylene glycol ($M_w = 20\,\mathrm{kg\,mol^{-1}}$) and 1.6 mM ADP. The reaction was started by illumination with a 50 W green LED lamp or a 5 W microscope light. Aliquots of 25 µL were taken at the beginning every 1 minutes and later on every 5 minutes from the reaction mixtures and the reaction was stopped by addition of the same volume of trichloroacetic acid (40 g/L). The ATP concentration was measured with the luciferin/luciferase assay and calibrated by addition of 10 µL ATP (7.8 µM) after each measurement.

Isolation and reactivation of flagella with light-driven energy module

Axonemes were isolated from wild-type *Chlamydomonas reinhardtii* cells, strain SAG 11-32b. They were grown axenically in TAP (tris-acetate-phosphate) medium on a 12 h/12 h day-night cycle. Flagella were isolated using dibucaine,(36, 37) then purified on a 25% sucrose cushion, and demembranated using detergent NP-40 in HMDEK solution supplemented with 0.2 mM Pefabloc. The membrane-free axonemes were resuspended in HMDEK buffer plus 1% (w/v) polyethylene glycol ($M_w = 20\,\mathrm{kg\,mol^{-1}}$), 0.2 mM Pefabloc, 20% sucrose and stored at −80 °C. To perform reactivation experiments, we thawed axonemes at room temperature and kept them on ice and used them for up to 2 hours. Next, we diluted axonemes in HMDEKP reactivation buffer (HMDEK plus 1 % PEG) which contains light-driven energy module and is supplemented with 0.2 mM Pefabloc. We infuse them into 100 µm deep flow chambers, built from cleaned glass and double-sided tape.

4.1 Axoneme contour tracking

We imaged reactivated axonemes using phase-contrast microscopy (100X objective, imaging frequency of 1000 fps). To increase the signal to noise ratio, we first inverted phase-contrast images and then subtracted the mean-intensity of the time series. This background-subtraction method increased the signal to noise ratio by a factor of three (32). Next, we applied a Gaussian filter to smooth the images. Tracking of axonemes is done using gradient vector flow (GVF) technique (33, 34). For the first frame, we select a region of interest that should contain only one actively beating axoneme. Then, we initialize the snake by drawing a line polygon along the contour of the axoneme in the first frame (see Fig. S5). This polygon is interpolated at N equally spaced points and used as a starting parameter for the snake. The GVF is calculated using the GVF regularization coefficient $\mu = 0.1$ with 20 iterations. The snake is then deformed according to the GVF where we have adapted the original algorithm by Xu and Prince for open boundary conditions. We obtain positions of N points along the contour length s of the filament so that $s = 0$ is the basal end and $s = L$ is the distal side, where L is the total contour length of filament. The position of filament at s_i is denoted by $r(s_i) = (x(s_i), y(s_i))$.

4.2 Mode analysis

We used the Frenet equations to analyze axoneme's shapes in a plane (35):

$$\frac{d\mathbf{r}(s)}{ds} = \hat{\mathbf{t}}(s) \qquad \text{and} \qquad \frac{d\hat{\mathbf{t}}(s)}{ds} = \kappa(s)\hat{\mathbf{n}}(s). \tag{1}$$

Here $\hat{\mathbf{t}}(s)$ is the unit tangent vector to the axoneme, $\hat{\mathbf{n}}(s)$ is the unit normal vector and $\kappa(s)$ is the curvature (see Fig. 3A). We define $\theta(s)$ to be the angle between the tangent vector at contour length s and the x-axis, then $\kappa(s) = d\theta(s)/ds$. Note that we rotate and translate the axoneme such that point $s = 0$ (basal end) is at position $(x, y) = (0, 0)$ and the local tangent vector at $s = 0$ is in the $\hat{x}$ direction, giving $\theta(0) = 0$. Following Stephens et al.(35), we performed principal mode analysis by calculating the covariance matrix of angles

$\theta(s)$ defined as $C(s,s') = \langle(\theta(s) - \langle\theta\rangle)(\theta(s') - \langle\theta\rangle)\rangle$. We then calculated the eigenvalues λ_n and the corresponding eigenvectors $V_n(s)$ of this matrix, showing that superposition of 4 eigenvectors corresponding to four largest eigenvalues can describe the axoneme's shape with high accuracy,

$$\theta(s,t) \approx \sum_{n=1}^{4} a_n(t) V_n(s). \tag{2}$$

Here the four variables $a_1(t), .., a_4(t)$ are the amplitudes of motion along different principal components and are given by $a_n(t) = \sum_s V_n(s)\theta(s)$.

5 Acknowledgment

R.A., E.B. and A.G. acknowledge support from the European Union's Horizon 2020 research and innovation programme under grant agreement MAMI No. 766007. C.K., A.B., E.B., K.S., T.V.K., and A.G. thank MaxSynBio Consortium, which is jointly funded by the Federal Ministry of Education and Research of Germany and the Max Planck Society. A. G. and R. A. thank M. Lorenz and the Göttingen Algae Culture Collection (SAG) for providing the *Chlamydomonas reinhardtii* strain 11-32b.

Author contributions: A.G. and T.V.K. designed the project. R.A. and A.G. isolated flagella and C.K., and T.V.K. built the energy module. R.A. and C.K. integrated the energy and motility unit. R.A., C.K., Y.S., S.G.P. and A.G. analyzed the data. A. G. performed the mode analysis of axonemes and A.B. wrote the Matlab code to track the axonemes. All the authors discussed the results and R.A., C.K., T.V.K. and A.G. wrote the manuscript.

Competing interests: The authors declare that they have no competing financial interests.

References

(1) L. Otrin, C. Kleineberg, L. Caire da Silva, K. Landfester, I. Ivanov, M. Wang, C. Bednarz, K. Sundmacher, and T. Vidaković-Koch. "Artificial organelles for energy regeneration". In: *Advanced Biosystems* 3.6 (2019), p. 1800323.

(2) K. Göpfrich, I. Platzman, and J. P. Spatz. "Mastering complexity: towards bottom-up construction of multifunctional eukaryotic synthetic cells". In: *Trends in biotechnology* 36.9 (2018), pp. 938–951.

(3) P. Schwille, J. Spatz, K. Landfester, E. Bodenschatz, S. Herminghaus, V. Sourjik, T. J. Erb, P. Bastiaens, R. Lipowsky, A. Hyman, et al. "MaxSynBio: avenues towards creating cells from the bottom up". In: *Angewandte Chemie International Edition* 57.41 (2018), pp. 13382–13392.

(4) D. Fletcher. *Which biological systems should be engineered?* 2018.

(5) D. Pantaloni, C. Le Clainche, and M.-F. Carlier. "Mechanism of actin-based motility". In: *Science* 292.5521 (2001), pp. 1502–1506.

(6) T. D. Pollard and G. G. Borisy. "Cellular motility driven by assembly and disassembly of actin filaments". In: *Cell* 112.4 (2003), pp. 453–465.

(7) J. R. Blake and M. A. Sleigh. "Mechanics of ciliary locomotion". In: *Biological Reviews* 49.1 (1974), pp. 85–125.

(8) T. Ishikawa. "Axoneme structure from motile cilia". In: *Cold Spring Harbor perspectives in biology* 9.1 (2017), a028076.

(9) Z. Carvalho-Santos, J. Azimzadeh, J. B. Pereira-Leal, and M. Bettencourt-Dias. "Tracing the origins of centrioles, cilia, and flagella". In: *J Cell Biol* 194.2 (2011), pp. 165–175.

(10) P. Satir and S. T. Christensen. "Overview of structure and function of mammalian cilia". In: *Annu. Rev. Physiol.* 69 (2007), pp. 377–400.

(11) D. Nicastro, C. Schwartz, J. Pierson, R. Gaudette, M. E. Porter, and J. R. McIntosh. "The molecular architecture of axonemes revealed by cryoelectron tomography". In: *Science* 313.5789 (2006), pp. 944–948.

(12) G. J. Pazour, N. Agrin, J. Leszyk, and G. B. Witman. "Proteomic analysis of a eukaryotic cilium". In: *The Journal of cell biology* 170.1 (2005), pp. 103–113.

(13) T. Yagi, K. Uematsu, Z. Liu, and R. Kamiya. "Identification of dyneins that localize exclusively to the proximal portion of Chlamydomonas flagella". In: *Journal of cell science* 122.9 (2009), pp. 1306–1314.

(14) I. Milisav. "Dynein and dynein-related genes". In: *Cell motility and the cytoskeleton* 39.4 (1998), pp. 261–272.

(15) I. Gibbons. "Studies on the adenosine triphosphatase activity of 14 S and 30 S dynein from cilia of Tetrahymena". In: *Journal of Biological Chemistry* 241.23 (1966), pp. 5590–5596.

(16) K. Ogawa and H. Mohri. "Studies on flagellar ATPase from sea urchin spermatozoa. I. Purification and some properties of the enzyme". In: *Biochimica et Biophysica Acta (BBA)-Bioenergetics* 256.1 (1972), pp. 142–155.

(17) L. Otrin, N. Marui, C. Bednarz, T. Vidakovic-Koch, I. Lieberwirth, K. Landfester, and K. Sundmacher. "Toward artificial mitochondrion: mimicking oxidative phosphorylation in polymer and hybrid membranes". In: *Nano letters* 17.11 (2017), pp. 6816–6821.

(18) C. Kleineberg, C. Wölfer, A. Abbasnia, D. Pischel, C. Bednarz, I. Ivanov, T. Heitkamp, M. Börsch, K. Sundmacher, and T. Vidakovic-Koch. "Light-driven ATP regeneration in diblock/grafted hybrid vesicles". In: *ChemBioChem* (2020).

(19) G. Steinberg-Yfrach, J.-L. Rigaud, E. N. Durantini, A. L. Moore, D. Gust, and T. A. Moore. "Light-driven production of ATP catalysed by F 0 F 1-ATP synthase in an artificial photosynthetic membrane". In: *Nature* 392.6675 (1998), pp. 479–482.

(20) J.-L. Rigaud, B. Pitard, and D. Levy. "Reconstitution of membrane proteins into liposomes: application to energy-transducing membrane proteins". In: *Biochimica et Biophysica Acta (BBA)-Bioenergetics* 1231.3 (1995), pp. 223–246.

(21) S. Matuschka, K. Zwicker, T. Nawroth, and G. Zimmer. "ATP synthesis by purified ATP-synthase from beef heart mitochondria after coreconstitution with bacteriorhodopsin". In: *Archives of biochemistry and biophysics* 322.1 (1995), pp. 135–142.

(22) P. Richard and P. Gräber. "Kinetics of ATP synthesis catalyzed by the H+-ATPase from chloroplasts (CF0F1) reconstituted into liposomes and coreconstituted with bacteriorhodopsin". In: *European journal of biochemistry* 210.1 (1992), pp. 287–291.

(23) B. Pitard, P. Richard, M. Duñach, and J.-L. Rigaud. "ATP synthesis by the F0F1 ATP synthase from thermophilic Bacillus PS3 reconstituted into liposomes with bacteriorhodopsin: 2. Relationships between proton motive force and ATP synthesis". In: *European journal of biochemistry* 235.3 (1996), pp. 779–788.

(24) T. E. Miller, T. Beneyton, T. Schwander, C. Diehl, M. Girault, R. McLean, T. Chotel, P. Claus, N. S. Cortina, J.-C. Baret, et al. "Light-powered CO2 fixation in a chloroplast mimic with natural and synthetic parts". In: *Science* 368.6491 (2020), pp. 649–654.

(25) K. Y. Lee, S.-J. Park, K. A. Lee, S.-H. Kim, H. Kim, Y. Meroz, L Mahadevan, K.-H. Jung, T. K. Ahn, K. K. Parker, et al. "Photosynthetic artificial organelles sustain and control ATP-dependent reactions in a protocellular system". In: *Nature biotechnology* 36.6 (2018), pp. 530–535.

(26) S. Berhanu, T. Ueda, and Y. Kuruma. "Artificial photosynthetic cell producing energy for protein synthesis". In: *Nature communications* 10.1 (2019), pp. 1–10.

(27) R. R. Ishmukhametov, M. A. Galkin, and S. B. Vik. "Ultrafast purification and reconstitution of His-tagged cysteine-less Escherichia coli F1Fo ATP synthase". In: *Biochimica Et Biophysica Acta (BBA)-Bioenergetics* 1706.1-2 (2005), pp. 110–116.

(28) D. Oesterhelt. "Isolation of the cell membrane of Halobacterium halobium and its fractionation into red and purple membrane". In: *Methods Enzymol.* 31 (1974), pp. 667–678.

(29) S. Fischer and P. Gräber. "Comparison of ΔpH-and Δφ-driven ATP synthesis catalyzed by the H+-ATPases from Escherichia coli or chloroplasts reconstituted into liposomes". In: *FEBS letters* 457.3 (1999), pp. 327–332.

(30) N. WAGNER, M. GUTWEILER, R. PABST, and K. DOSE. "Coreconstitution of bacterial ATP synthase with monomeric bacteriorhodopsin into liposomes: A comparison between the efficiency of monomeric bacteriorhodopsin and purple membrane patches in coreconstitution experiments". In: *European journal of biochemistry* 165.1 (1987), pp. 177–183.

(31) V. F. Geyer, P. Sartori, B. M. Friedrich, F. Jülicher, and J. Howard. "Independent control of the static and dynamic components of the Chlamydomonas flagellar beat". In: *Current Biology* 26.8 (2016), pp. 1098–1103.

(32) V. Geyer. "Characterization of the flagellar beat of the single cell green alga *Chlamydomonas reinhardtii*". PhD thesis. Sächsische Landesbibliothek-Staats-und Universitätsbibliothek Dresden, 2013.

(33) C. Xu and J. L. Prince. “Gradient vector flow: A new external force for snakes”. In: *IEEE Proc. CVPR*. IEEE. July 1997, pp. 66–71. ISBN: 0-8186-7822-4. DOI: 10.1109/CVPR.1997.609299.

(34) C. Xu and J. L. Prince. “Snakes, shapes, and gradient vector flow”. In: *IEEE Transactions on image processing* 7.3 (1998), pp. 359–369.

(35) G. J. Stephens, B. Johnson-Kerner, W. Bialek, and W. S. Ryu. “Dimensionality and dynamics in the behavior of C. elegans”. In: *PLoS computational biology* 4.4 (2008).

(36) G. B. Witman. “Isolation of Chlamydomonas flagella and flagellar axonemes”. In: *Meth. Enzymology*. Vol. 134. Elsevier, 1986, pp. 280–290.

(37) J. Alper, V. Geyer, V. Mukundan, and J. Howard. “Reconstitution of flagellar sliding”. In: *Meth. Enzymology*. Vol. 524. Elsevier, 2013, pp. 343–369.

6 Supplementary Information

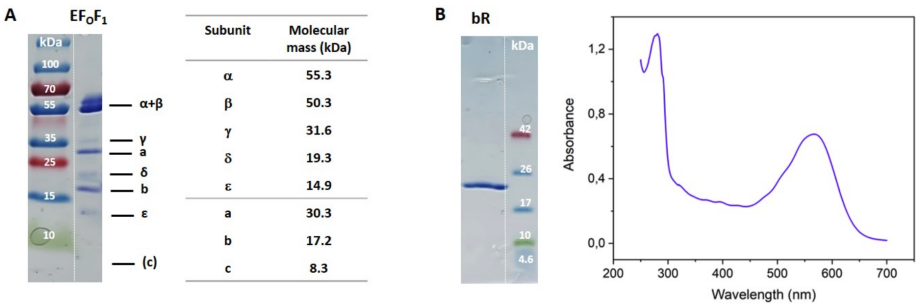

Subunit	Molecular mass (kDa)
α	55.3
β	50.3
γ	31.6
δ	19.3
ε	14.9
a	30.3
b	17.2
c	8.3

Fig. 1: SDS-PAGE of purified proteins. (A) Coomassie-stained SDS-PAGE of purified EF_OF_1-ATP synthase and molecular masses of EF_OF_1 subunits. (B) Coomassie-stained SDS-PAGE of purified bR with the corresponding absorbance spectrum.

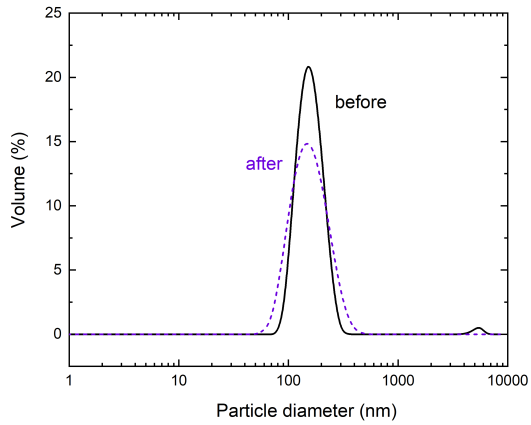

Fig. 2: Size distribution of vesicles before (before) and after reconstitution and removal of detergent using Bio Beads (after).

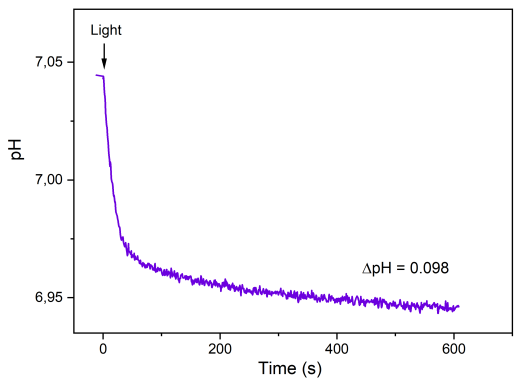

Fig. 3: Proton pumping of bR as measured by encapsulated pyranine.

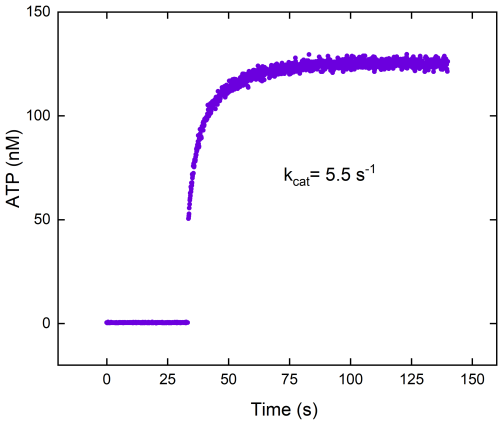

Fig. 4: Turnover (k_{cat}) of ATP synthase as determined in an acid-base transition experiment.

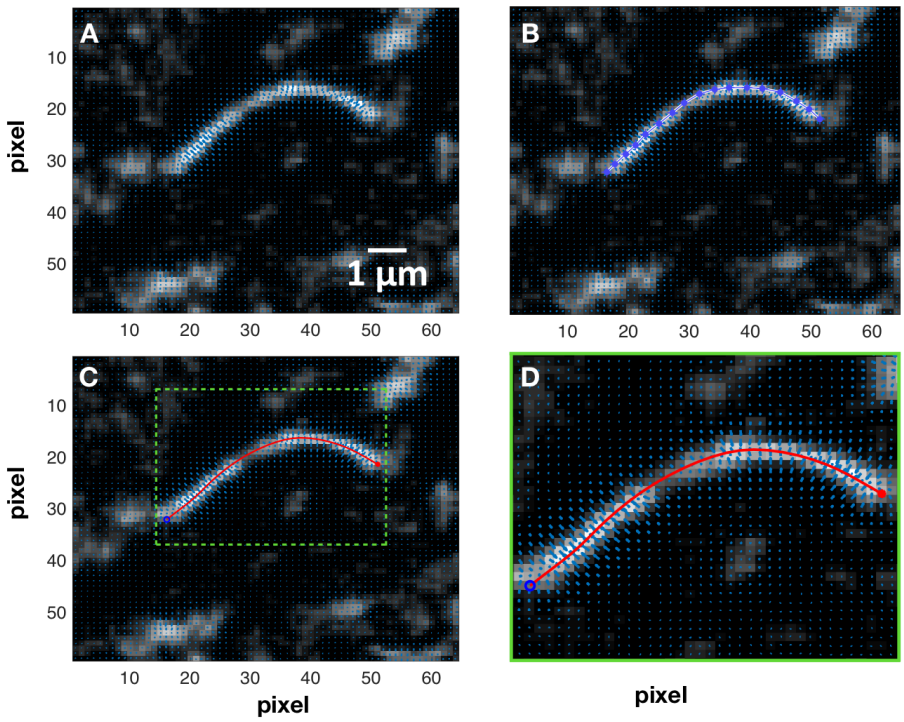

Fig. 5: A) Gradient vector flow calculated at the vicinity of an axoneme. B) The initial selection of a polygon for the first frame which deforms according to the gradient vector flow. C) The final tracked shape of an axoneme. D) A zoomed-in image showing the gradient vector flow (blue arrows) at a higher magnification.